Supplementary Materials for

Metabolic signaling directs the reciprocal lineage decisions of αβ and γδ T cells

Kai Yang, Daniel Bastardo Blanco, Xiang Chen, Pradyot Dash, Geoffrey Neale, Celeste Rosencrance, John Easton, Wenan Chen, Changde Cheng, Yogesh Dhungana, Anil KC, Walid Awad, Xi-Zhi J. Guo, Paul G. Thomas, and Hongbo Chi*

.

*Corresponding author. E-mail: hongbo.chi@stjude.org

This PDF file includes:

Materials and Methods

Flow cytometry

For analysis of surface markers, cells were stained in PBS containing 2% (wt/vol) BSA, with anti-CD4 (RM4-5), anti-CD8α (53-6.7), anti-TCRβ (H57-597), anti-CD25 (PC61.5), anti-CD44 (1M7), anti-CD62L (MEL-14), anti-CD45.1 (A20), anti-CD45.2 (104), anti-TCRγδ (eBioGL3), anti-CD24 (M1/69), anti-CD73 (eBioTY/11.8), anti-CD5 (53-7.3), anti-CD98 (RL388), and anti-CD71 (R17217). Intracellular Ki67 (SolA15), phospho-S6 (D57.2.2E), and phospho-4E-BP1 (236B4) were analyzed by flow cytometry according to the manufacturer's instructions. Two antibodies (C-20, Santa Cruz Biotechnology; and D16D10, Cell Signaling Technology) were used to measure ID3 expression by flow cytometry, with similar results. For measurement of ROS, mitochondrial mass and potential, thymocytes were incubated in the medium containing 10 μM CM-H2DCFDA (5-(and-6)-chloromethyl-2,7-dichlorodihydrofluorescein diacetate acetyl ester; Life Technologies), 10 nM MitoTracker Deep Red (Life Technologies) or 20 nM TMRM (tetramethyl rhodamine, methyl ester; ImmunoChemistry Technologies), respectively, for 30 min at 37°C before staining surface markers. BrdU incorporation was measured in thymocytes from mice injected with BrdU (1 mg/mouse) for 3 h according to manufacturer's instructions (BD Biosciences). Caspase-3 activity was measured using active caspase-3 apoptosis kit (BD Biosciences). Flow cytometry data were acquired on LSRII or LSR Fortessa (Becton Dickinson), and analyzed using FlowJo software (Tree Star).

Cell purification and cultures

Lineage-negative WT and *Rptor*$^{-/-}$ DN3 (CD4^{-}CD8^{-}TCRγδ^{-}TCRβ^{-}CD25^{hi}CD44^{-}) or DN3a cells (CD4^{-}CD8^{-}TCRγδ^{-}TCRβ^{-}CD25^{hi}CD44^{-}CD28^{-}) were sorted on a MoFlow (Beckman-Coulter) or

Reflection (i-Cyt). DN3 cells were used for Seahorse assay and *in vitro* cultures with OP9 or OP9-DL1 cells in the presence of IL-7 (0.5 ng/ml) and Flt3L (5 ng/ml) for 3 days. For metabolic perturbation, DN3a cells were co-cultured with OP9-DL1 cells in the presence of rapamycin (10 ng/ml), DCA (10 mM), galactose (0.5 mM) and galactose oxidase (GAO, 0.3 U/ml), GSH (5 mM), or NAC (20 mM) for 3-5 days. For T cell differentiation under a stromal cell-free culture condition (*38*), sorted DN3a cells were cultured in DLL4 (2 μg/ml)-coated plates, in the presence of CXCL12 (100 ng/ml) or IL-7 (1 ng/ml) to promote αβ or γδ T cell development, respectively, with or without the indicated inhibitors for 4 days.

Gene expression profiling by microarray analysis

RNA samples from freshly isolated ISP (WT, $n = 4$; *Rptor*$^{-/-}$, $n = 3$), DN3a, or γδ T cells (WT, $n = 3$; *Rptor*$^{-/-}$, $n = 3$) were analyzed with the Affymetrix Mouse Gene 2.0 ST GeneChip array. Gene set enrichment analysis (GSEA) within hallmark gene sets (MSigDB) or canonical pathways (MSigDB c2.CP gene sets for canonical pathways) was performed as described (*22*). Differentially expressed transcripts were identified by ANOVA (Partek Genomics Suite v6.5) and the Benjamini-Hochberg method was used to estimate the false discovery rate (FDR) as described previously (*53*). Lists of differentially expressed genes by > 0.5 $\log_2$ difference or more were analyzed using Ingenuity Pathway Analysis (Qiagen, Inc.) for upstream transcription regulators.

RNA and immunoblot analysis

Real-time PCR analysis was performed with primers and probe sets from Applied Biosystems as described (*53*). Immunoblots were performed as described (*56*) using the following antibodies: EGR1 (44D5), RAPTOR (24C12), p-ERK (9101), ID3 (D16D10), p-p65 (all from Cell Signaling

Technology), β-ACTIN (AC-15; Sigma); ATP5A, UQCRC2, MTCO1, SDHB, and NDUFB8 (using total OXPHOS antibody cocktail from Abcam).

Metabolic assays

OCR and ECAR were measured in XF media (non-buffered DMEM containing 5 mM glucose, 2 mM L-glutamine and 1 mM sodium pyruvate), under basal conditions and in response to 1 μM oligomycin, 2 μM fluoro-carbonyl cyanide phenylhydrazone (FCCP) and 1 μM Rotenone using the XF-24 Extracellular Flux Analyzer (Seahorse Bioscience). For glycolytic rate, the various subsets of thymocytes were cultured in Click's medium containing 1 μCi [3-^{3}H]-glucose for 6 h. Glycolytic flux was determined by measuring the detritiation of [3-^{3}H]-glucose, as we previously described (*30*).

Statistical analysis for biological experiments

P values were calculated by two-tailed Mann-Whitney test, two-tailed unpaired Student's *t* test, or ANOVA using GraphPad Prism, unless otherwise noted. *P* value of < 0.05 was considered significant. All error bars represent the s.e.m.

Single-cell multiplex RT-PCR and sequencing of TCRγ chains

Thymocytes from WT or *Rptor*$^{-/-}$ mice were harvested and resuspended. After depletion of CD4^{+} cells using CD4 (L3T4) MicroBeads (Miltenyi Biotec), the remaining cells were stained with anti-CD4, anti-CD8, anti-NK1.1, anti-TCRβ, anti-TCRγδ, anti-Ter119, anti-B220 and anti-Gr1 in 200 μl of sorting buffer (PBS containing 0.1% BSA, Fraction V (Gibco)) on ice, in dark for 20 min. Following staining, cells were washed three times and resuspended in sorting buffer (containing

200 units of RNAsin/ml (Promega)) and filtered through 40 μM cell strainer prior to sorting. γδ T cells (TCRγδ^{+}CD4^{-}CD8^{-}NK1.1^{-}TCRβ^{-}B220^{-}Ter119^{-}Gr1^{-}) were sorted singly into each well of a 384-well plate (Eppendorf) using an iCyt Synergy cell sorter (Sony) with the following parameters: Multi-drop sort OFF, Multi-drop exclude OFF, Division 10, Center sort %: 90. At least one column of the 384-well plates was left unsorted to use as negative controls for PCR. After sorting, the plates were sealed using plate sealer film (MicroAmp, Applied Biosystems) and centrifuged at 500 g for 3 min and stored at -80°C until further amplification. Unbiased amplification of TCRγ chain at the single cell level was carried out as per method described before (*24*). Briefly, the cDNA synthesis was performed directly from single cells without any RNA extraction step using the SuperScript VILO cDNA synthesis kit (Thermo Scientific) in a volume of 1 μl of reaction mix (0.2 μl of 5× VILO reaction mix, 0.1 μl of 10× SuperScript® Enzyme mix, 0.1 μl of 1% Triton X-100 (Sigma)). Following reverse transcription, a multiplex nested PCR was carried out using a Taq polymerase based PCR kit (Qiagen). The protocol for the first and second round PCR (except for the primer components), sequencing, and data analysis were performed as previously described (*24, 25*). The primers for the mouse TCRγ chain were used as below.

Name	**External**	**Internal**
TRGV1-3 For	GCAGCTGGAGCAAACTG	CTGAATTATCGGTCACCAG
TRGV4 For	CAAATATCCTGTAAAGTTTTCATC	GTTTAGAGTTTCTATTATATGTCCTTGCAAC
TRGV5 For	GATATCTCAGGATCAGCTCTCC	TACCCGAAGACCAAACAAGAC
TRGV6 For	TCACCTCTGGGGTCATATG	AGAGGAAAGGAAATACGGC
TRGV7 For	CAACTTGGAAGAAAGAATAATGTC	CACCAAGCTAGAGGGGTC
TRGC Rev	CTTTTCTTTCCAATACACCC	TCDGGAAAGAACTTTTCAAGG

Single-cell RNA sequencing (scRNA-Seq)

Lineage-negative thymocytes (Ter119$^-$Gr1$^-$CD19$^-$NK1.1$^-$CD4$^-$CD8$^-$TCRβ$^-$TCRγδ$^-$CD44$^-$; representative of DN3-DN4 cells) were sorted into culture medium, spun down, and re-suspended in 100 μl of 1× PBS + 0.04% BSA. The cells were counted and examined for viability using a Luna Dual Florescence Cell Counter (Logos Biosystems). Single-cell suspensions were loaded onto the Chromium Controller according to their respective cell counts to generate 6000 single-cell GEMs (gel beads in emulsion) per sample. Each sample was loaded into a separate channel. Libraries were prepared using the Chromium Single Cell 3' v2 Library and Gel Bead Kit (10x Genomics). The cDNA content of each sample after cDNA amplification of 12 cycles was quantified and quality checked using a High-Sensitivity DNA chip with a 2100 Bioanalyzer (Agilent Technologies) to determine the number of PCR amplification cycles to yield sufficient library for sequencing. After library quantification and quality check by DNA 1000 chip (Agilent Technologies), samples were diluted to 3.5 nM for loading onto the HiSeq 4000 (Illumina) with a 2 × 75 Paired-end kit using the following read length: 26 bp Read1, 8 bp i7 Index, and 98 bp Read2. An average of 400,000,000 reads per sample was obtained (~approximately 80,000 reads per cell),

Analysis for scRNA-Seq data

Alignment, barcode assignment, and UMI counting

The Cell Ranger 1.3 Single-Cell Software Suite (10x Genomics) was implemented to process the raw sequencing data from the Illumina HiSeq run. This pipeline performed de-multiplexing, alignment (mm10), and barcode processing to generate gene-cell matrices used for downstream analysis. Specifically, data for 2 WT and 3 *Rptor*$^{-/-}$ samples were combined, and UMIs mapped to genes encoding ribosomal proteins were removed. Cells with low (bottom 2.5%, potentially dead

cells with broken membrane) or high (top 2.5%, potentially two or more cells in a single droplet) UMI counts were filtered. On average, 4,123 mRNA molecules (UMIs) were captured in a cell (median: 3,448, range: 1,703–9,999), representing 2,110 genes (median: 1,968, range: 59 – 3,916). The expression level of each gene is normalized to 10,000 UMIs per cell and log transformed by adding 0.25 to the expression matrix.

Clustering

The subpopulation structure of the whole dataset was inferred using Latent Cellular State Analysis (LCA), a novel clustering algorithm developed in house for analyzing large-scale scRNA-Seq data (manuscript in preparation). Briefly, LCA first used singular value decomposition (SVD) to derive latent cellular states from the expression matrix for individual cells. The number of significant cellular states was determined using the Tracy-Widom test on eigenvalues. A modified version of spectral clustering was performed on the significant cellular states of individual cells (cellular states explained by total UMIs ignored) with different number of clusters (2-30). The optimal number of clusters was manually selected from top models determined by the silhouette measure for solutions with different number of clusters.

Data visualization

Underneath cell variations were visualized in a 2D projection by t-distributed stochastic neighbor embedding (tSNE). Expression of individual genes or pathway scores were color coded (gray: not expressed; from low to high: blue-green-yellow-red) for each cell on tSNE plots.

Generation of gene signatures and statistical analysis for over-representation

We generated DN3a signature from the genes specifically expressed in DN3a but not in DN3b, DN3b-DN4 or DN4 cells (92 genes with FDR < 0.05, $\log_2$ fold change > 1.5 for each comparison) (*47*) (GSE15907). The pre-TCR signaling signature was generated from genes upregulated in DN3b cells compared with DN3a cells (75 genes with FDR < 0.05, $\log_2$ fold change > 2) (GSE15907). The γδ T cell gene signature was generated from genes selectively expressed by γδ T cells *(48)* (121 genes upregulated in γδ T cells, but not DN3b cells, as compared with DN3a cells, with FDR < 0.05, $\log_2$ fold change > 2). For gene signatures of metabolic and signaling pathways, the list of 2,088 genes with strong and dynamic expression in thymocyte differentiation (*47*) was used to intersect with gene sets from MSigDB (hallmark mTORC1 signaling, hallmark MYC targets v1, hallmark glycolysis, KEGG NOTCH signaling pathway, and PDGF ERK DN.V1 DN) for refined gene signatures relevant to thymocyte development. For scRNA-Seq analysis, genes from these signatures were retained if they were expressed in at least 10% of cells in any cluster. Gene signature activity was calculated as the average value for all retained genes. Relative over-representation of gene signatures for a specific cluster (**Fig. 6D**) was determined using one-tailed Mann-Whitney test (cells in a specific cluster vs all other cells). Differential activity of a gene signature or individual gene expression between defined clusters was determined using two-tailed Mann-Whitney test.

Pseudo-temporal analysis

Monocle 2 (*49*) was used to generate the single cell pseudo-temporal trajectories with default settings.

Statistical analysis for WT and Rptor$^{-/-}$ enrichment for individual clusters

The numbers of cells in and outside a specific cluster were counted for each mouse. Logistic regression was used to assess the association between the cluster cell counts and the independent predictor of WT and *Rptor*$^{-/-}$ samples (**Fig. 6E**).

Fig. S1

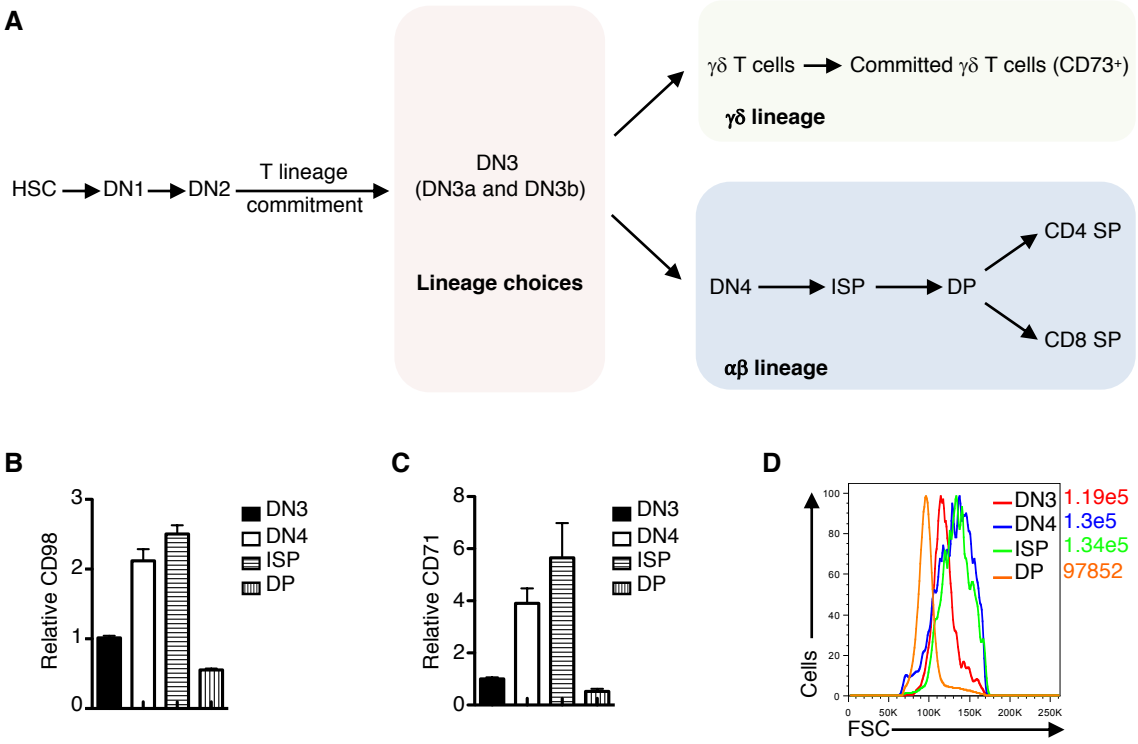

Fig. S1. Dynamic regulation of nutrient transporters and cell growth in developing thymocytes. (**A**) Diagram of T cell development in the thymus. Hematopoietic stem cells (HSC) derived from the bone marrow migrate to the thymus and progress through well-defined developmental stages to become αβ or γδ T cells. Double-negative cells (DN, without expression of CD4 and CD8) at early thymocyte development can be divided into four stages, with the DN3 stage being a crucial checkpoint for T cell lineage choices. DN3 cells with successful β-selection continue their developmental process by transitioning through the DN4, ISP (immature single-positive) and DP (double-positive) stages before becoming CD4 or CD8 single-positive cells (SP). Alternatively, DN3 cells complete γδ-selection to become γδ T cells, followed by induction of CD73 expression to mark fully committed γδ T cells. (**B** and **C**) Relative expression of CD98 (B) and CD71 (C) (MFI in DN3 cells is set to 1) in thymocyte subsets. (**D**) Plot of cell size (FSC) in thymocyte subsets. Data are representative of at least five independent experiments (B to D).

Fig. S2

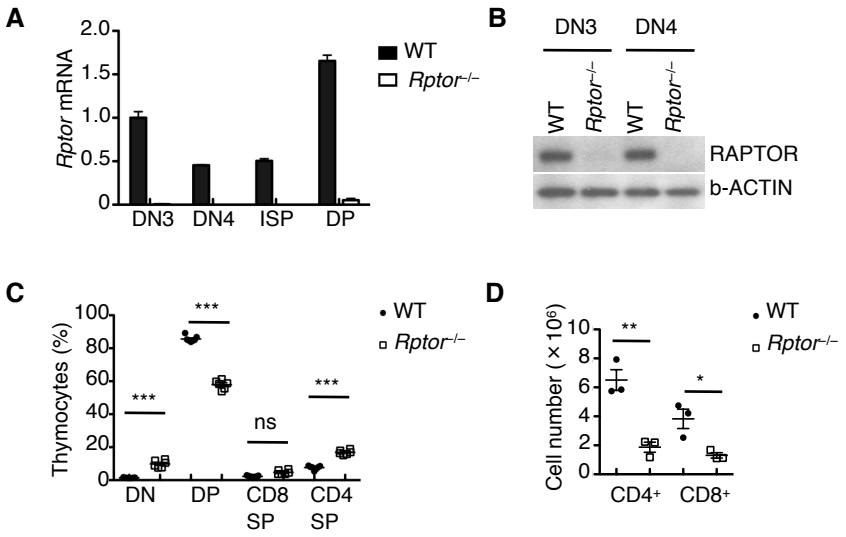

Fig. S2. mTOR signaling is required for thymocyte development. (**A** and **B**) Analysis of RAPTOR mRNA (A) and protein (B) expression in thymocyte subsets from WT and *Rptor*$^{-/-}$ mice. (**C**) Frequencies of thymocyte subsets from WT and *Rptor*$^{-/-}$ mice. Each symbol represents an individual mouse (WT, $n = 8$; *Rptor*$^{-/-}$, $n = 5$). (**D**) Cellularity of CD4$^+$ and CD8$^+$ T cells in the spleen of WT and *Rptor*$^{-/-}$ mice. Each symbol represents an individual mouse ($n = 3$ each group). Data are mean ± s.e.m. ns, not significant; *$P < 0.05$, **$P < 0.005$, and ***$P < 0.0001$. One-way ANOVA with Tukey test (C), or two-tailed unpaired *t*-test (D). Data are representative of at least three independent experiments (A to D).

Fig. S3

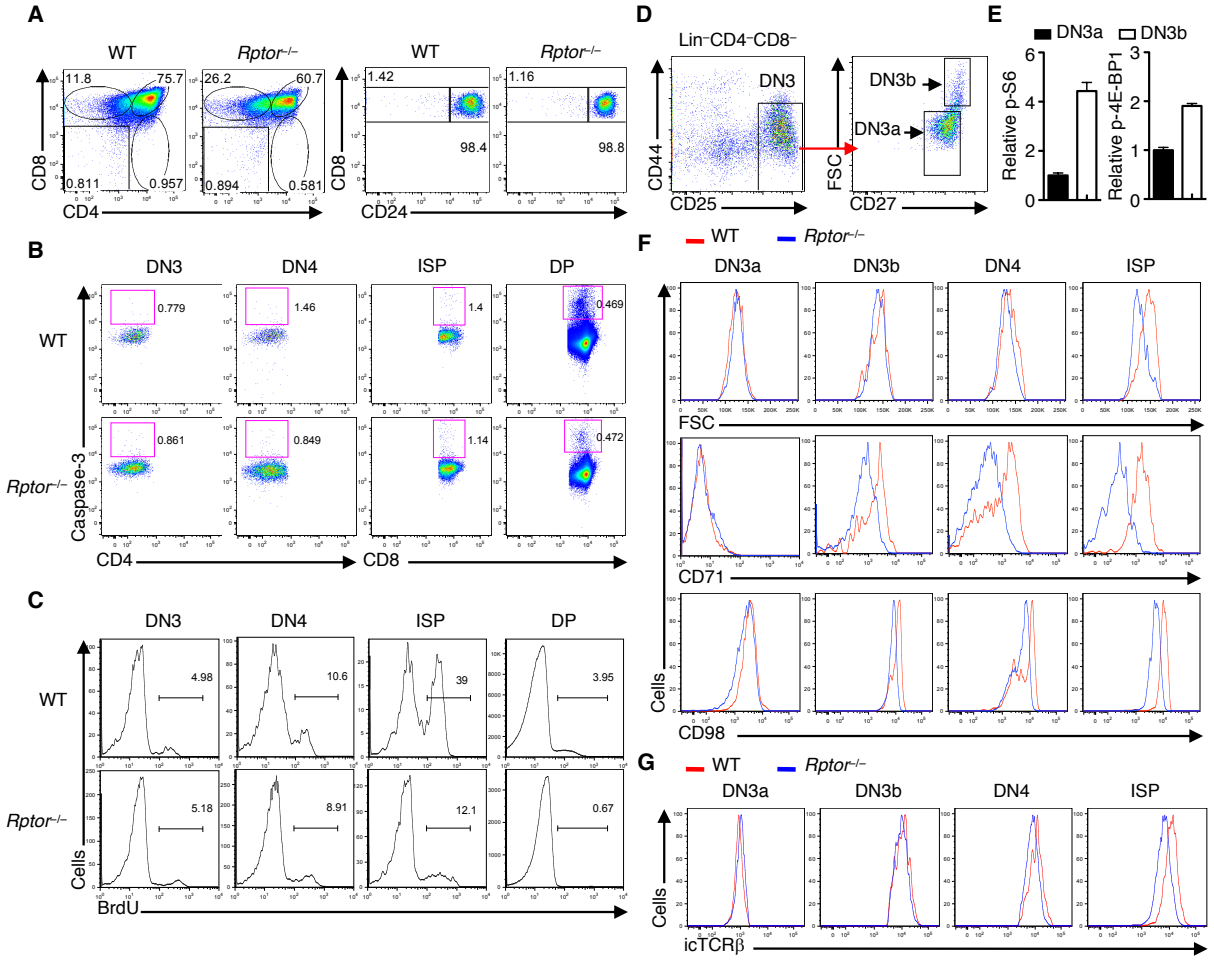

Fig. S3. RAPTOR deficiency diminishes differentiation, proliferation, and nutrient transporter expression of ISP cells, but not cell survival. (**A**) ISP cells from WT and *Rptor*$^{-/-}$ mice were cultured with OP9-DL1 cells for 1 day, followed by analysis of CD4 and CD8 (left panel) and CD24 and CD8 expression on CD4^{-}CD8^{+} ISP cells (right panel). (**B**) Caspase-3 activity in thymocyte subsets in WT and *Rptor*$^{-/-}$ mice. (**C**) BrdU incorporation in thymocyte subsets in WT and *Rptor*$^{-/-}$ mice pulsed with BrdU for 3 h. (**D**) Gating strategy for DN3a (Lin^{-}CD4^{-}CD8^{-}CD25^{+}CD44^{-}CD27^{-}) and DN3b (Lin^{-}CD4^{-}CD8^{-}CD25^{+}CD44^{-}CD27^{+}) cells. (**E**) Relative phosphorylation of S6 and 4E-BP1 (MFI in DN3a cells is set to 1) in DN3a and DN3b cells from WT mice. (**F** and **G**) Plots of FSC, CD71 and CD98 (F), and icTCRβ (G) in thymocyte subsets in WT and *Rptor*$^{-/-}$ mice. Data are mean ± s.e.m. Data are representative of at least three independent experiments (A to G). Numbers indicate percentage of cells in gates.

Fig. S4

A

Hallmark gene sets	NES	FDR q-val
HALLMARK_MTORC1_SIGNALING	-2.704	<0.001
HALLMARK_MYC_TARGETS_V1	-2.608	<0.001
HALLMARK_MYC_TARGETS_V2	-2.476	<0.001
HALLMARK_OXIDATIVE_PHOSPHORYLATION	-2.256	<0.001
HALLMARK_TNFA_SIGNALING_VIA_NFKB	-2.231	<0.001
HALLMARK_CHOLESTEROL_HOMEOSTASIS	-2.174	<0.001
HALLMARK_UNFOLDED_PROTEIN_RESPONSE	-1.885	5.43E-04
HALLMARK_UV_RESPONSE_UP	-1.874	4.75E-04
HALLMARK_FATTY_ACID_METABOLISM	-1.801	0.001095
HALLMARK_E2F_TARGETS	-1.689	0.004129
Canonical pathway gene sets	**NES**	**FDR q-val**
REACTOME_M_G1_TRANSITION	-2.470	<0.001
REACTOME_AMYLOIDS	-2.451	<0.001
REACTOME_RNA_POL_I_PROMOTER_OPENING	-2.409	<0.001
REACTOME_INFLUENZA_LIFE_CYCLE	-2.380	<0.001
REACTOME_CHOLESTEROL_BIOSYNTHESIS	-2.360	<0.001
REACTOME_RESPIRATORY_ELECTRON_TRANSPORT_ATP_SYNTHESIS_ BY_CHEMIOSMOTIC_COUPLING_AND_HEAT_PRODUCTION_BY_UNCOUPLING_PROTEINS_	-2.347	<0.001
REACTOME_SYNTHESIS_OF_DNA	-2.344	<0.001
REACTOME_S_PHASE	-2.334	<0.001
REACTOME_TCA_CYCLE_AND_RESPIRATORY_ELECTRON_TRANSPORT	-2.298	<0.001
REACTOME_ASSEMBLY_OF_THE_PRE_REPLICATIVE_COMPLEX	-2.296	<0.001

B

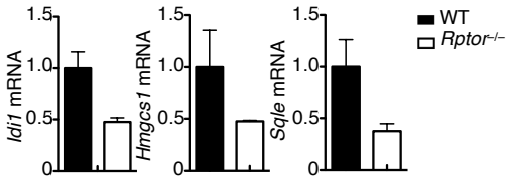

C

Upstream regulators	*P*-value
MYC	1.23E-20
FOXO1	2.79E-14
CREB1	3.66E-14
SREBF2	5.16E-13
SREBF1	1.37E-11
TRIM24	1.93E-09
MYCN	4.42E-06
PPARGC1B	1.71E-05
HNF4A	2.11E-05
ATF4	2.65E-05

Fig. S4. RAPTOR controls metabolic gene expression programs in thymocytes. (**A**) List of the top 10 downregulated gene sets in the databases of hallmarks and canonical pathways (MSigDB) in *Rptor*$^{-/-}$ ISP cells, as identified by gene set enrichment assay (GSEA) of microarray profiles (WT, $n = 4$; *Rptor*$^{-/-}$, $n = 3$). NES, normalized enrichment score; FDR, false discovery rate. No significantly upregulated gene sets (FDR < 0.05) were identified in these databases. (**B**) Analysis of *Idi1*, *Hmgcs1* and *Sqle* mRNA expression in WT and *Rptor*$^{-/-}$ ISP cells. (**C**) List of the top 10 potential transcription regulators downregulated in *Rptor*$^{-/-}$ ISP cells as identified by Ingenuity Pathway Analysis (IPA) of microarray profiles (WT, $n = 4$; *Rptor*$^{-/-}$, $n = 3$). Data are one experiment (A, C), or representative of three independent experiments (B).

Fig. S5

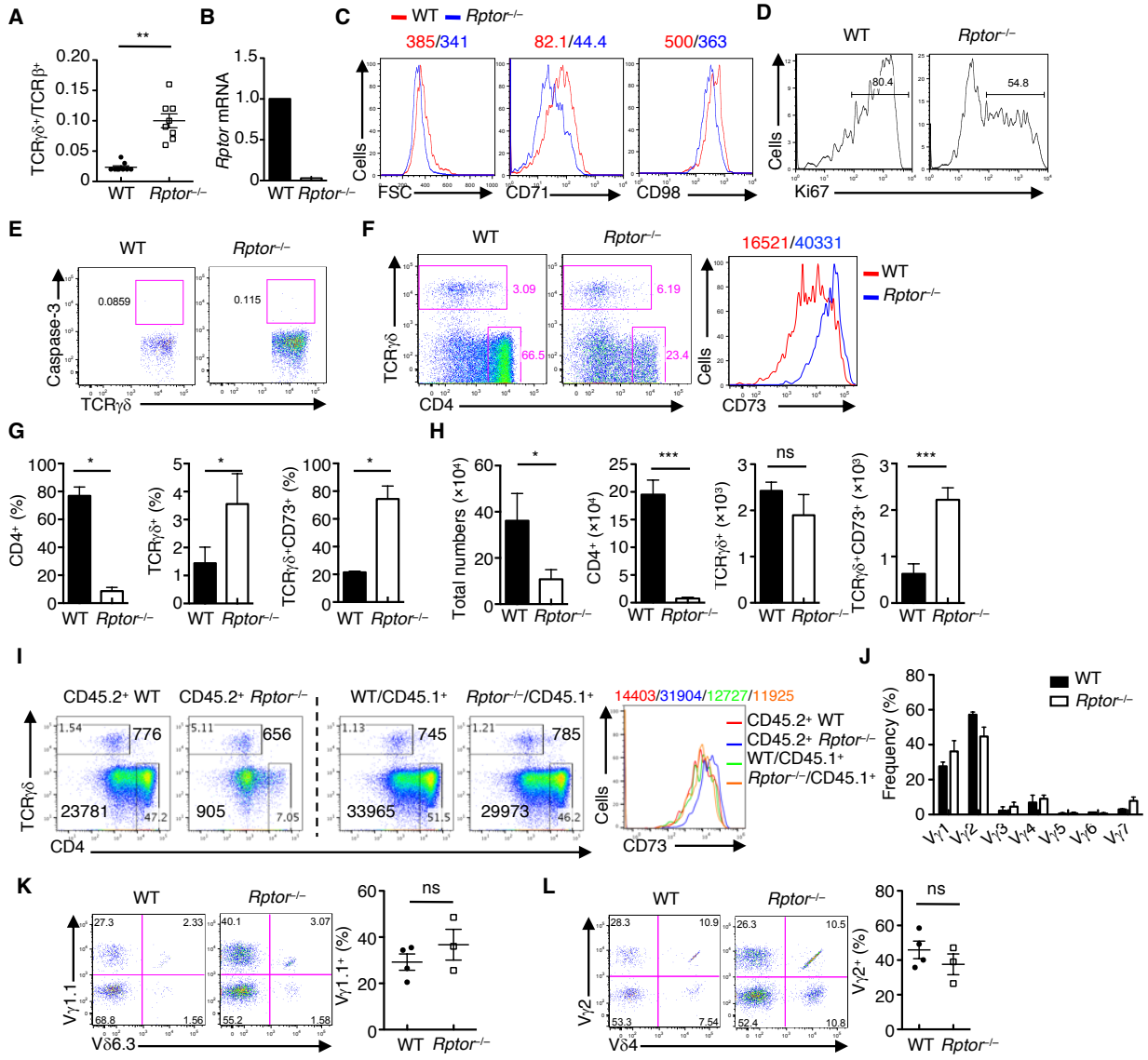
A
B
C
D
E
F
G
H
I
J
K
L
WT
Rptor−/−
TCRγδ+/TCRβ+
Rptor mRNA
385/341
82.1/44.4
500/363
FSC
CD71
CD98
Cells
Ki67
80.4
54.8
Caspase-3
TCRγδ
0.0859
0.115
CD4
CD73
3.09
66.5
6.19
23.4
16521/40331
CD4+ (%)
TCRγδ+ (%)
TCRγδ+CD73+ (%)
Total numbers (×10⁴)
CD4+ (×10⁴)
TCRγδ+ (×10³)
TCRγδ+CD73+ (×10³)
ns
CD45.2+ WT
CD45.2+ Rptor−/−
WT/CD45.1+
Rptor−/−/CD45.1+
14403/31904/12727/11925
776
656
745
785
23781
47.2
905
7.05
33965
51.5
29973
46.2
Frequency (%)
Vγ1
Vγ2
Vγ3
Vγ4
Vγ5
Vγ6
Vγ7
Vγ1.1
Vδ6.3
Vγ1.1+ (%)
Vδ4
Vγ2+ (%)

Fig. S5. RAPTOR deficiency impacts γδ T cell development. (**A**) Ratio of TCRγδ$^+$ to TCRβ$^+$ cells in WT and *Rptor*$^{-/-}$ mice. Each symbol represents an individual mouse (n = 8 each group). (**B**) Analysis of *Rptor* mRNA in WT and *Rptor*$^{-/-}$ TCRγδ$^+$ cells (*Rptor* mRNA in WT is normalized to 1). (**C**) Plots of FSC, CD71 and CD98 in WT and *Rptor*$^{-/-}$ TCRγδ$^+$ cells, with MFI plotted above graphs. (**D**) Plot of Ki67 expression in WT and *Rptor*$^{-/-}$ TCRγδ$^+$ cells. Numbers indicate the frequency of the Ki67$^+$ population. (**E**) Caspase-3 activity of WT and *Rptor*$^{-/-}$ TCRγδ$^+$ cells. (**F**) WT or *Rptor*$^{-/-}$ cells were cultured with OP9-DL1 cells, followed by examination of CD4$^+$ and TCRγδ$^+$ T cells (left), and CD73 expression on TCRγδ$^+$ cells with MFI plotted above the graph (Right). (**G, H**) Frequencies (G) and numbers (H) of total cells, CD4$^+$ T cells, TCRγδ$^+$ cells, and committed γδ T cells (TCRγδ$^+$CD73$^+$) in F. (**I**) WT (CD45.2$^+$) or *Rptor*$^{-/-}$ (CD45.2$^+$) DN3a cells were cultured with CD45.1$^+$ DN3a cells in the presence of OP9-DL1 cells, followed by examination of TCRγδ$^+$ and CD4$^+$ T cells, with cell numbers included in the graphs (left). Right, expression of CD73 on TCRγδ$^+$ cells with MFI plotted above the graph. (**J**) Single cell analysis of diverse TCRγ chains expressed in thymic TCRγδ$^+$ T cells of WT and *Rptor*$^{-/-}$ mice. The Vγ usage derived from the CDR3γ sequence data is plotted. (**K** and **L**) Flow cytometry of Vγ1.1$^+$Vδ6.3$^+$ (K) and Vγ2$^+$Vδ4$^+$ (L) TCRγδ$^+$ T cell subsets in the thymus. Right, frequency of Vγ1.1$^+$ or Vγ2$^+$ cells. Each symbol represents an individual mouse (WT, n = 4; *Rptor*$^{-/-}$, n = 3). Data are mean ± s.e.m. ns, not significant; *$P < 0.05$; **$P < 0.01$, ***$P < 0.001$. Two-tailed unpaired t-test (A), or two-tailed Mann-Whitney test (G, J to L), or one-tailed unpaired t-test (H). Data are representative of at least three independent experiments (A, C to I), or two independent experiments (B, J to L). Numbers indicate percentage of cells in the quadrants or gates.

Fig. S6

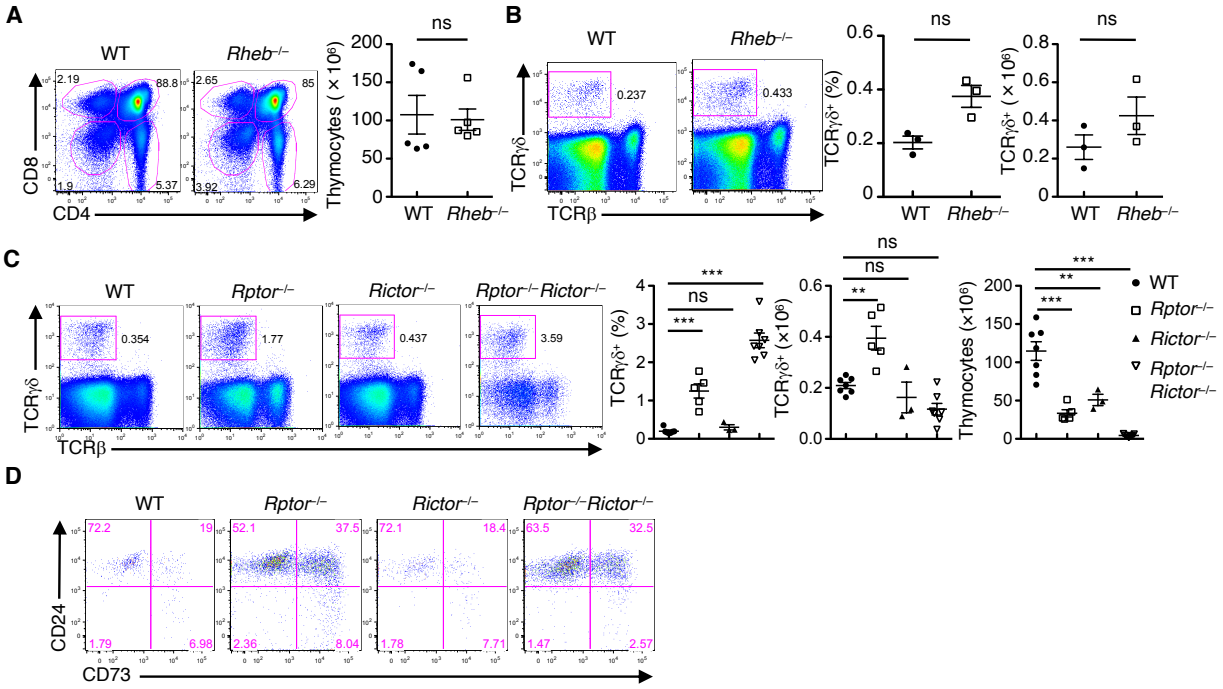

Fig. S6. Loss of RHEB or RICTOR does not affect the development of γδ T cells. (**A**) Flow cytometry of thymocyte subsets of WT and *Rheb*$^{-/-}$ mice (left). Right, cellularity of total thymocytes. Each symbol represents an individual mouse (n = 5 each group). (**B**) Flow cytometry of TCRγδ^{+} cells in WT and *Rheb*$^{-/-}$ mice. Frequency (middle) and cellularity (right) of TCRγδ^{+} cells in the thymus of WT and *Rheb*$^{-/-}$ mice (n = 3 each group). (**C**) Flow cytometry of TCRγδ^{+} cells in WT, *Rptor*$^{-/-}$, *Rictor*$^{-/-}$ and *Rptor*$^{-/-}$*Rictor*$^{-/-}$ thymocytes (left). Right, frequency and cellularity of TCRγδ^{+} cells and total thymocyte cellularity in the indicated mouse groups. Each symbol represents an individual mouse (WT, n = 7; *Rptor*$^{-/-}$, n = 5; *Rictor*$^{-/-}$, n = 3; *Rptor*$^{-/-}$*Rictor*$^{-/-}$, n = 7). (**D**) Flow cytometry of CD73 and CD24 expression on TCRγδ^{+} cells in the thymus from the indicated mice. Data are mean ± s.e.m. ns, not significant; $^{**}P < 0.001$, and $^{***}P < 0.0001$. Two-tailed unpaired t-test (A, B for cellularity analyses), two-tailed Mann-Whitney test (B for frequency analysis), or one-way ANOVA with Tukey test (C). Data are representative of two independent experiments (D), or at least three independent experiments (A to C). Numbers indicate percentage of cells in quadrants or gates.

Fig. S7

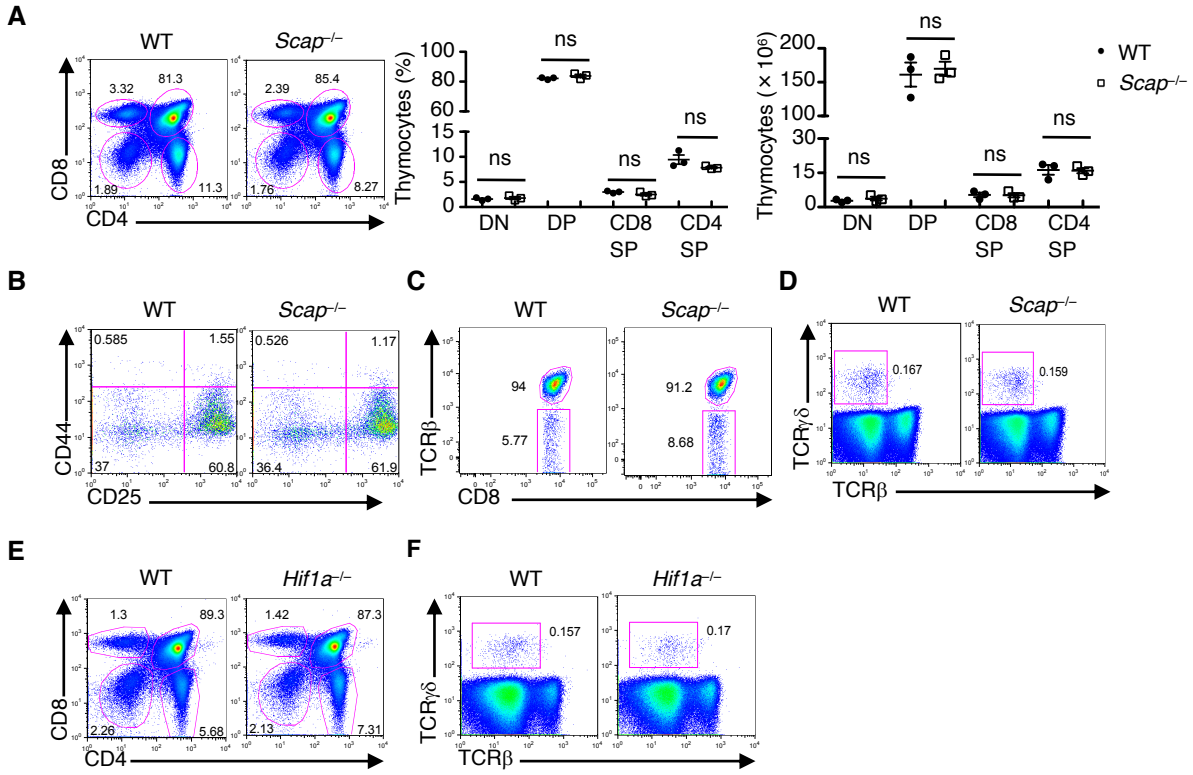

Fig. S7. SCAP and HIF1α are dispensable for T cell development. (**A** to **D**) Analysis of thymocyte development of WT and *Scap*$^{-/-}$ mice. (**A**) Flow cytometry (left) of thymocyte subsets in WT and *Scap*$^{-/-}$ mice. Frequencies (middle) and cellularity (right) of thymocyte subsets. Each symbol represents an individual mouse (n = 3 each group). (**B**) Flow cytometry of DN1-4 subsets (gated on lineage-negative DN cells) of WT and *Scap*$^{-/-}$ thymocytes. (**C**) Flow cytometry of ISP cells in WT and *Scap*$^{-/-}$ mice. (**D**) Flow cytometry of TCRγδ^{+} cells in WT and *Scap*$^{-/-}$ thymocytes. (**E** and **F**) Flow cytometry of thymocyte subsets (E), and TCRγδ^{+} cells (F) in the thymus of WT and *Hif1a*$^{-/-}$ mice. Data are mean ± s.e.m. ns, not significant. One-way ANOVA with Tukey test (A). Data are representative of two independent experiments (A to F). Numbers indicate percentage of cells in quadrants or gates.

Fig. S8

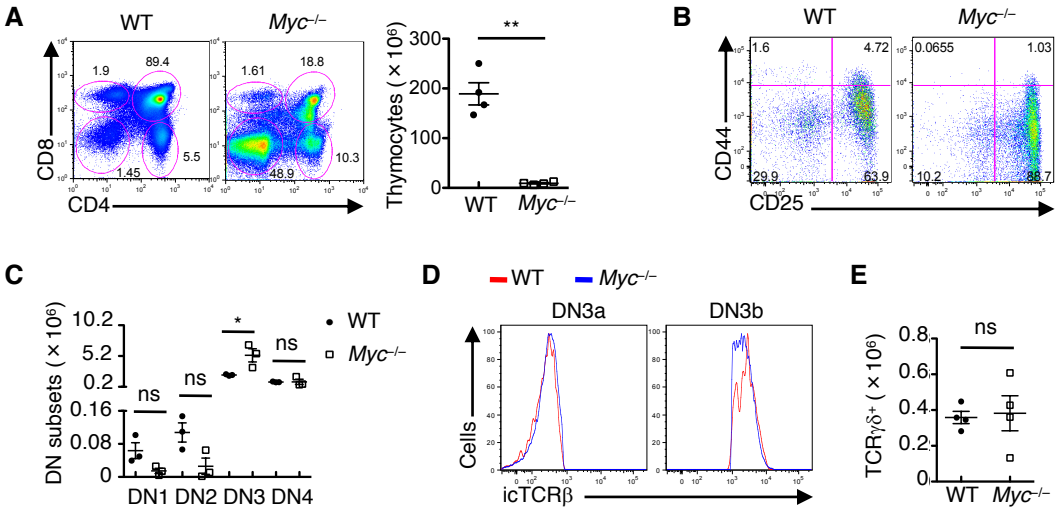

Fig. S8. MYC is implicated in αβ and γδ T cell development. (**A**) Flow cytometry of thymocyte subsets in WT and *Myc*$^{-/-}$ mice (left). Right, cellularity of total thymocytes. Each symbol represents an individual mouse ($n = 4$ each group). (**B**) Flow cytometry of DN1-4 subsets (gated on lineage-negative DN thymocytes) in WT and *Myc*$^{-/-}$ mice. (**C**) Cellularity of DN subsets in WT and *Myc*$^{-/-}$ thymocytes. Each symbol represents an individual mouse ($n = 3$ each group). (**D**) Plots of icTCRβ in the indicated WT and *Myc*$^{-/-}$ DN subsets. (**E**) Cellularity of TCRγδ^{+} cells in the thymus of WT and *Myc*$^{-/-}$ mice. Each symbol represents an individual mouse ($n = 4$ each group). Data are mean ± s.e.m. ns, not significant; $^{*}P < 0.05$, and $^{**}P < 0.005$. Two-tailed unpaired *t*-test (A, C, E). Data are representative of at least three independent experiments (A to E). Numbers indicate percentage of cells in quadrants or gates.

Fig. 9

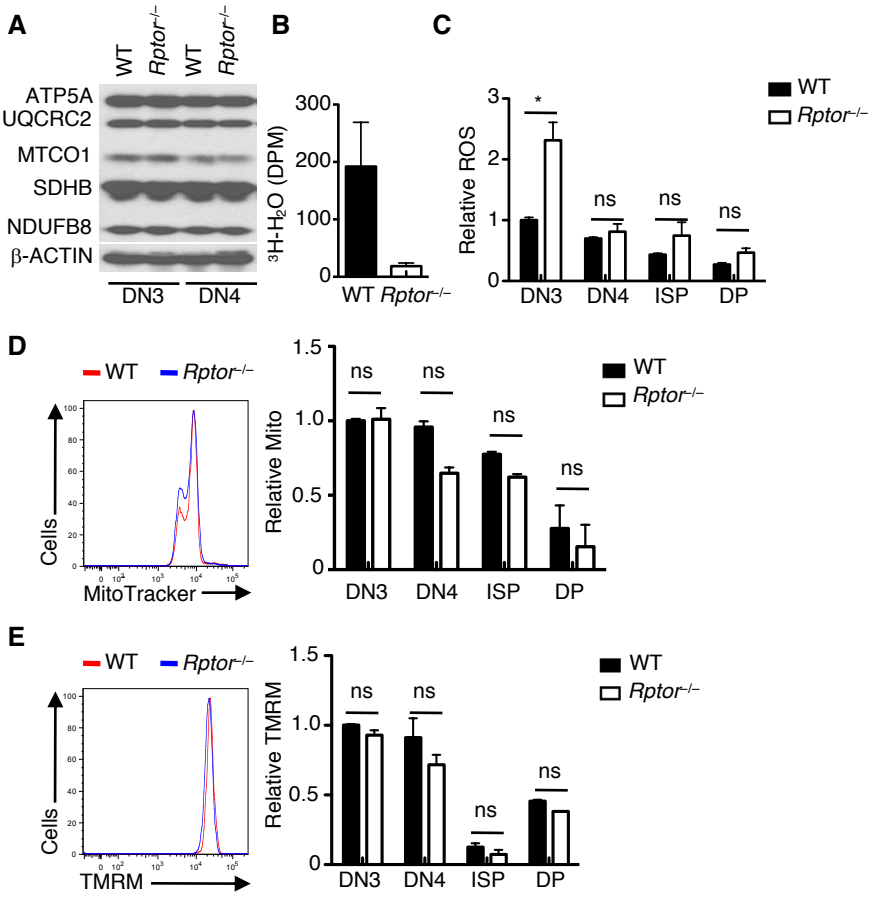

Fig. S9. RAPTOR-deficient DN3 cells exhibit increased ROS but normal mitochondrial mass and membrane potential. (**A**) The expression of proteins involved in OXPHOS in DN3 and DN4 cells of WT and *Rptor*$^{-/-}$ mice. (**B**) Measurement of glycolytic activity in WT and *Rptor*$^{-/-}$ DN3 cells. (**C**) Relative MFI of ROS in thymocyte subsets of WT and *Rptor*$^{-/-}$ mice (MFI of WT DN3 cells is set to 1). (**D** and **E**) Plots of MitoTracker (D) and TMRM (E) in thymocyte subsets in WT and *Rptor*$^{-/-}$ mice (left). Right, relative MFI of MitoTracker (Mito) (D) and TMRM (E) in thymocyte subsets of WT and *Rptor*$^{-/-}$ mice (MFI of WT DN3 cells is set to 1). Data are mean ± s.e.m. ns, not significant; *$P < 0.0001$. Two-way ANOVA with Bonferroni test (C to E). Data are representative of two independent experiments (A), or representative/combination of two independent experiments (B to E).

Fig.10

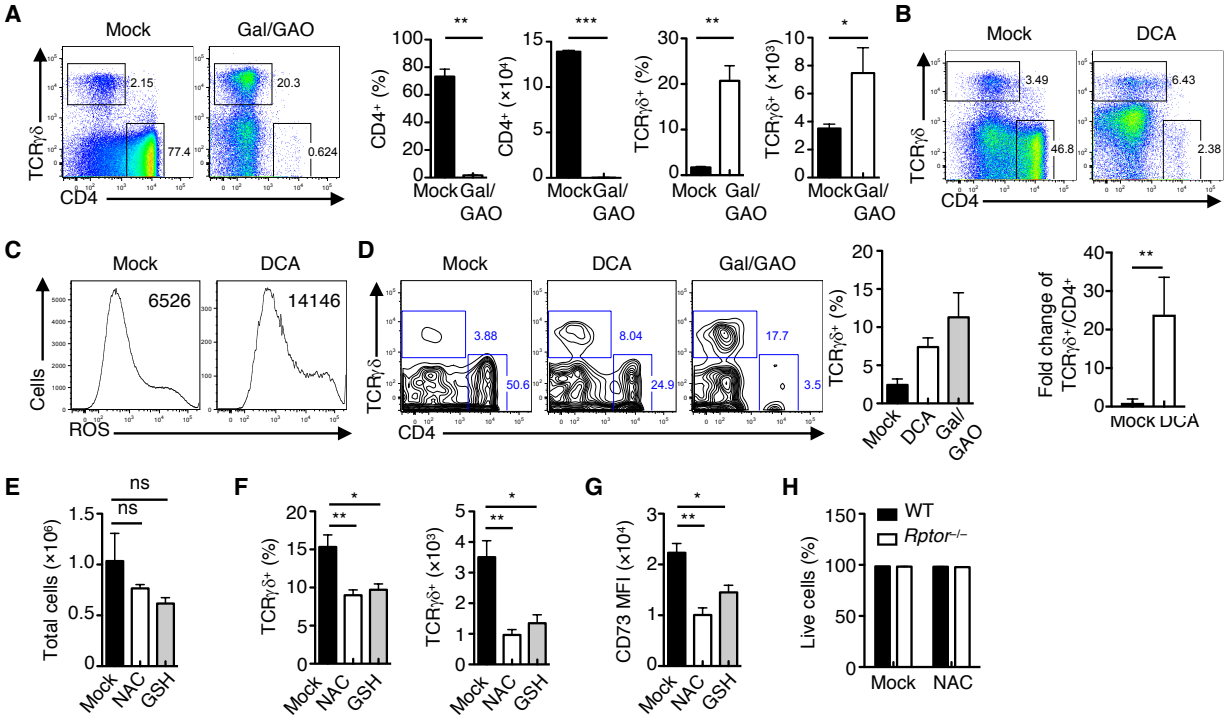

Fig. S10. Modulation of ROS production alters fate choices of DN3 cells. (**A**) WT DN3a cells were co-cultured with OP9-DL1 cells in the absence or presence of Gal/GAO, followed by analysis of TCRγδ and CD4 expression (left). Right, frequencies and numbers of $CD4^+$ and $TCR\gamma\delta^+$ cells (n = 5 each group). (**B**) WT DN3a cells were co-cultured with OP9-DL1 cells with or without DCA treatment, followed by analysis of TCRγδ and CD4 expression (upper). Lower: fold change of the ratio of $TCR\gamma\delta^+$ to $CD4^+$ cells (WT without DCA treatment is set to 1, n = 3 each group). (**C**) Analysis of ROS production in WT DN3a cells co-cultured with OP9-DL1 cells in the absence or presence of DCA for 3 days, with MFI plotted in graphs. (**D**) WT DN3a cells were cultured with plate-bound NOTCH ligand DLL4 in the presence of CXCL12 and treated with the indicated inhibitors, followed by examination of CD4 and TCRγδ expression (left). Right, frequency of $TCR\gamma\delta^+$ cells. (**E**) WT DN3a cells were co-cultured with OP9-DL1 cells in the absence or presence of NAC or GSH for 5 days, and analyzed for cellularity of total cells in the culture (n = 3 each group). (**F**) WT DN3a cells were cultured with plate-bound NOTCH ligand DLL4 in the presence of IL-7 and treated with either NAC or GSH, followed by examination of $TCR\gamma\delta^+$ frequency (left) and cellularity (right) (n = 4 each group). (**G**) MFI of CD73 on $TCR\gamma\delta^+$ cells in F. (**H**) WT and *Rptor*$^{-/-}$ DN3a cells were co-cultured with OP9-DL1 cells in the absence or presence of NAC for 3 days, followed by analysis of live cells ($7\text{-}AAD^-$ cells). Data are mean ± s.e.m. ns, not significant; $*P < 0.05$, $**P < 0.01$, $***P < 0001$. Two-tailed Mann-Whitney test (A), one-tailed unpaired t-test (B), or one-way ANOVA with Tukey test (D to G). Data are representative of at least three independent experiments (A to H). Numbers indicate percentage of cells in gates.

Fig. 11

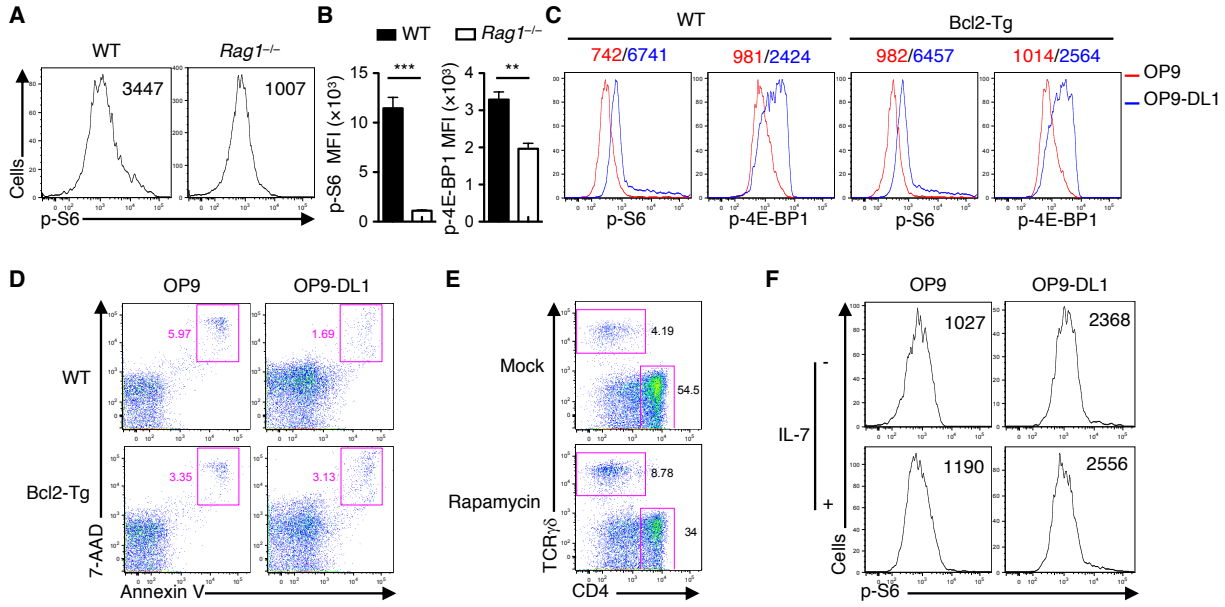

Fig. S11. mTORC1 activation integrates signals from pre-TCR and NOTCH. (**A**) Plots of p-S6 in DN3 cells from WT and *Rag1*$^{-/-}$ mice ($n = 3$ each group), with MFI plotted in graphs. (**B**) Phosphorylation of S6 and 4E-BP1 in WT and *Rag1*$^{-/-}$ DN3a cells co-cultured with OP9-DL1 cells in the absence of IL-7 for 2 days. (**C** and **D**) DN3a cells from WT or Bcl2-Tg mice were cultured with OP9 or OP9-DL1 cells in the absence of IL-7 for 2 days, followed by examination of phosphorylation of S6 and 4E-BP1 (C) and Annexin V and 7-AAD (D), with MFI plotted above graphs. (**E**) WT DN3 cells were co-cultured with OP9-DL1 cells in the absence or presence of rapamycin (10 ng/ml) for 3 days, followed by analysis of CD4 and TCRγδ. (**F**) WT DN3 cells were co-cultured with OP9 or OP9-DL1 cells in the absence or presence of IL-7 for 2 days, followed by analysis of p-S6, with MFI plotted in graphs. Data are mean ± s.e.m. $^{**}P < 0.005$, and $^{***}P < 0.001$. Two-tailed unpaired *t*-test (B). Data are representative of three (A, B, E, F), or two (C, D) independent experiments. Numbers indicate percentage of cells in gates.

Fig. S12

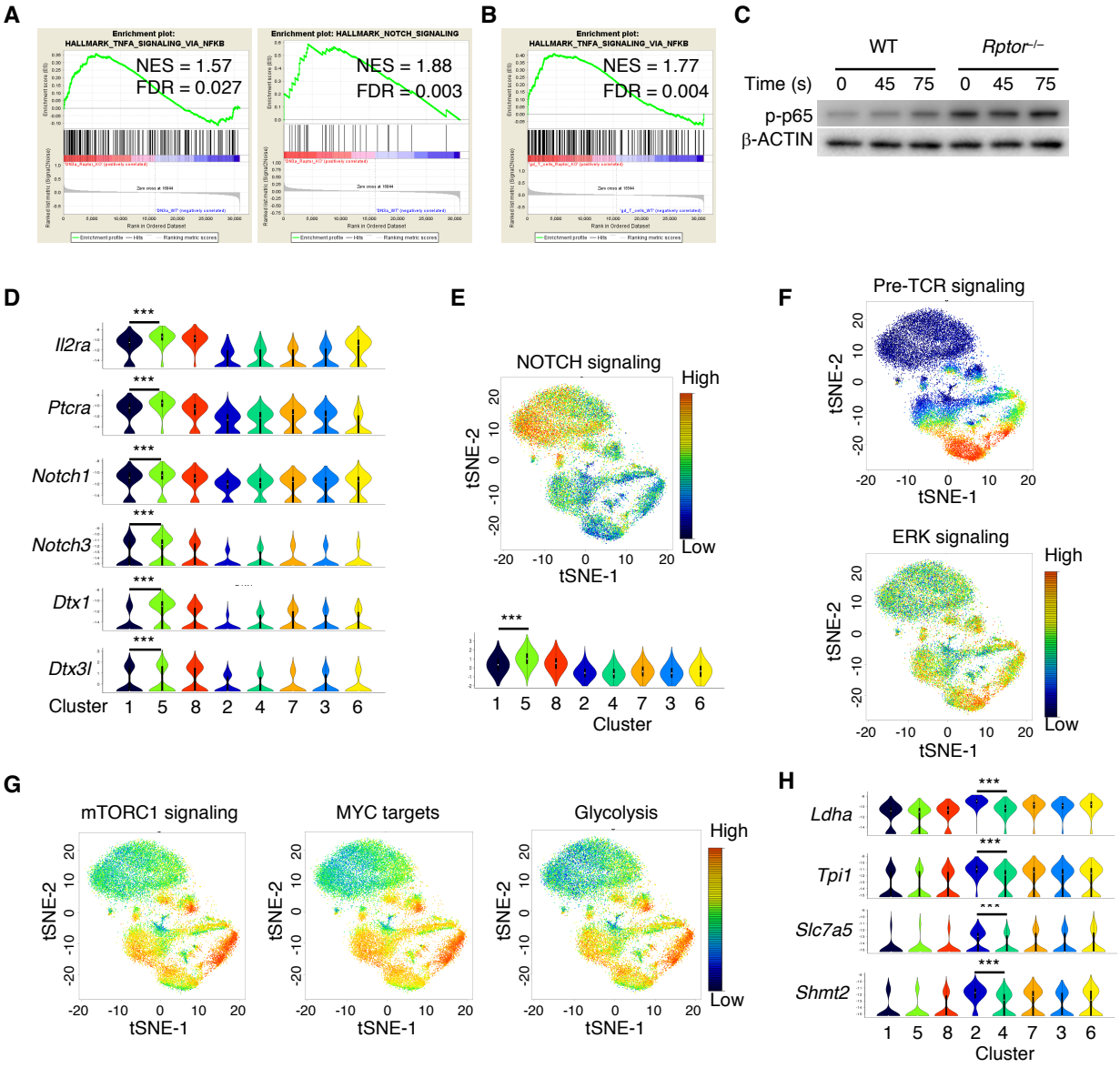
A
Enrichment plot: HALLMARK_TNFA_SIGNALING_VIA_NFKB
NES = 1.57
FDR = 0.027
Enrichment plot: HALLMARK_NOTCH_SIGNALING
NES = 1.88
FDR = 0.003
B
Enrichment plot: HALLMARK_TNFA_SIGNALING_VIA_NFKB
NES = 1.77
FDR = 0.004
C
WT
Rptor−/−
Time (s) 0 45 75 0 45 75
p-p65
β-ACTIN
D
Il2ra
Ptcra
Notch1
Notch3
Dtx1
Dtx3l
Cluster 1 5 8 2 4 7 3 6
E
NOTCH signaling
High
Low
tSNE-1
tSNE-2
Cluster
F
Pre-TCR signaling
ERK signaling
G
mTORC1 signaling
MYC targets
Glycolysis
H
Ldha
Tpi1
Slc7a5
Shmt2

Fig. S12. RAPTOR deficiency alters transcriptional programs and signaling and metabolic pathways. (**A** and **B**) GSEA reveals the significant enrichment of the upregulated pathways in RAPTOR-deficient DN3a cells (A) and γδ T cells (B). (**C**) Immunoblot analysis of p-p65 (S276) and β-ACTIN in WT and RAPTOR-deficient γδ T cells stimulated with anti-γδTCR for the indicated time points. (**D**) Violin plots of *Il2ra*, *Ptcra* and additional NOTCH target genes among the 8 clusters. A violin plot combines the box plot and the local density estimation into a single display. The black bars and thin lines within the violin plots indicate the interquartile range (1^{st} quantile – 3^{rd} quantile) and the entire range of the data (up to 1.5 fold of interquartile range from $1^{st}/3^{rd}$ quantile), respectively, and the white dots in the center indicate the median values. (**E**) tSNE (upper) and violin (lower) plots of the signature of NOTCH signaling among the 8 clusters. (**F**) tSNE plots of the signatures of pre-TCR and ERK signaling among the 8 clusters. (**G**) tSNE plots of gene signatures of mTORC1 signaling, MYC targets and glycolysis among the 8 clusters. (**H**) Violin plots of metabolic genes among the 8 clusters. Data are mean ± s.e.m. ***$P <$ 0.001. Two-tailed Mann-Whitney test (D, E, and H). Data are one experiment (A, B (WT, $n = 3$; *Rptor*$^{-/-}$, $n = 3$); D to H (WT, $n = 2$; *Rptor*$^{-/-}$, $n = 3$)), or representative of two (C) independent experiments.

Fig. S13

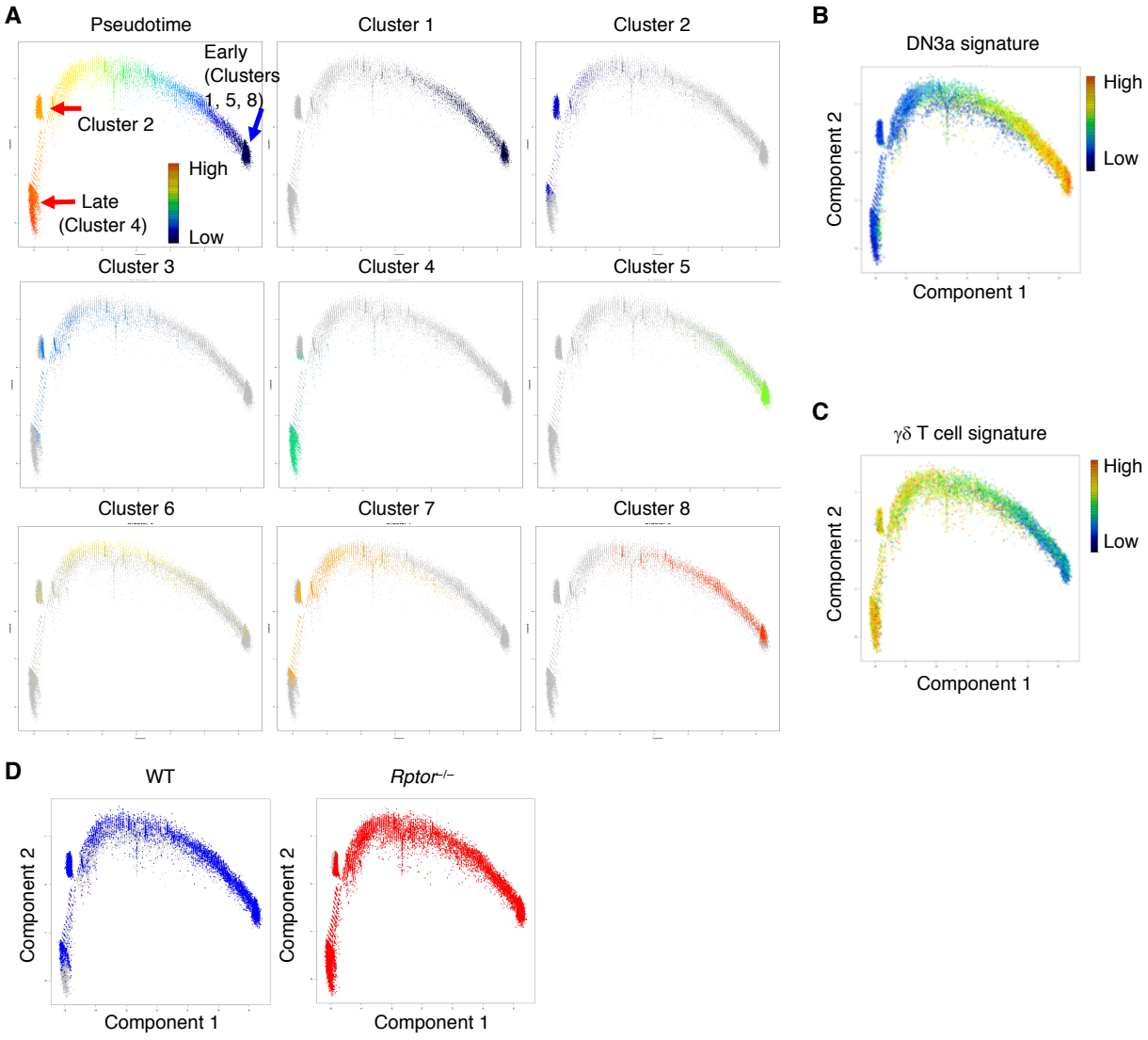

Fig. S13. Monocle 'pseudotime' trajectory of single cell transcriptomics data. (**A**) Upper left panel: pseudotime trajectory of scRNA-Seq data colorized by pseudotime (blue indicates early time, and red indicates late time). The remaining 8 panels are the cell projections for each individual cluster. (**B**) Projection of DN3a gene signature onto pseudotime trajectory. (**C**) Projection of γδ T cell gene signature onto pseudotime trajectory. (**D**) Pseudotime trajectory of cellular density colorized by genotypes: WT (blue) and *Rptor*$^{-/-}$ (red).

Fig. S14

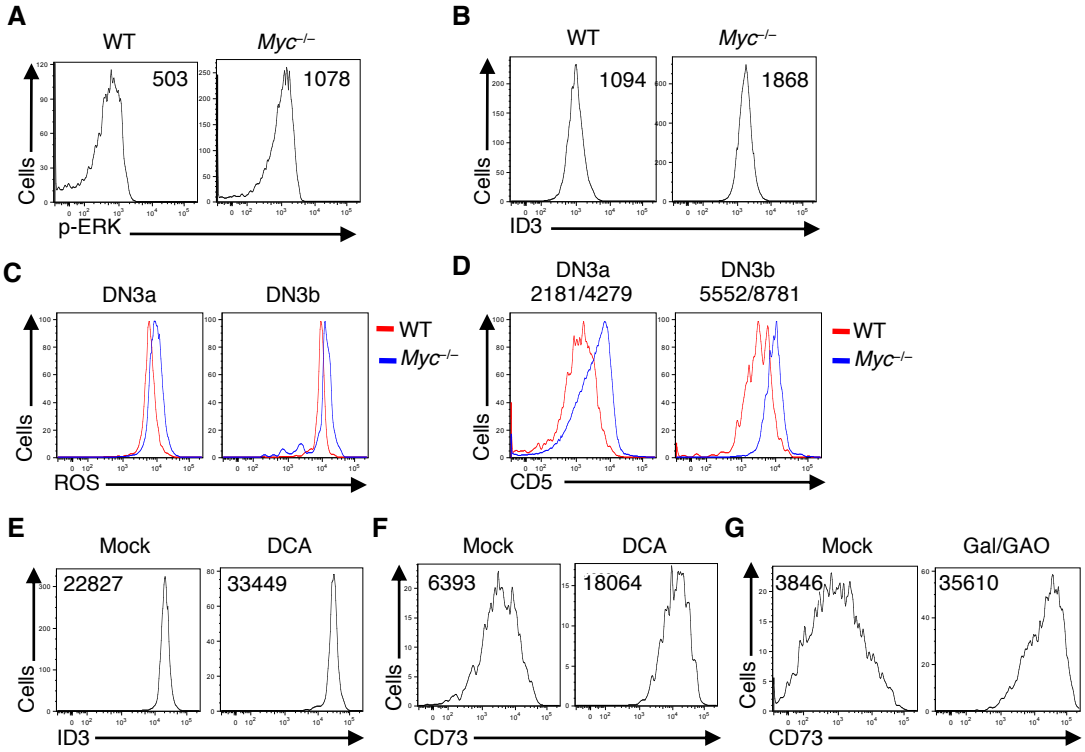

Fig. S14. Loss of RAPTOR or MYC enhances signal strength. (**A** and **B**) Plots of p-ERK (A) and expression of ID3 (B) in WT and *Myc*$^{-/-}$ DN3 cells, with MFI plotted in graphs. (**C** and **D**) Comparison of ROS production (C) and CD5 expression (D) between DN3 cell subsets from WT and *Myc*$^{-/-}$ mice. (**E**) WT DN3a cells were co-cultured with OP9-DL1 cells in the absence or presence of DCA (10 mM) for 3 days, followed by analysis of ID3 expression, with MFI plotted in graphs. (**F** and **G**) Expression of CD73 on TCRγδ^{+} cells from co-culture of WT DN3a cells with OP9-DL1 cells upon DCA (F) or Gal/GAO treatment (G), with MFI plotted in graphs. Data are representative of at least three independent experiments (A to G).

Fig. S15

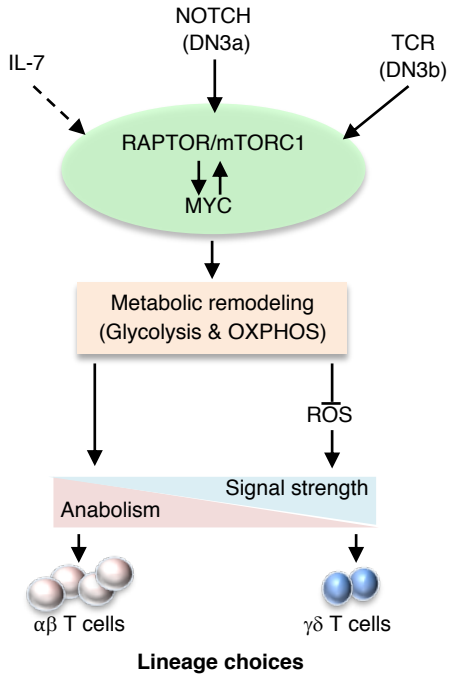

Fig. S15. Schematics of mTORC1 and metabolic control of redox homeostasis and signal strength in T cell lineage choices. mTORC1, activated by TCR and NOTCH signaling, intersects with MYC in a feed-forward manner to orchestrate cell metabolism in developing thymocytes. Dynamic metabolic remodeling, including proper engagement of glycolysis and OXPHOS, contributes to anabolism and cell expansion. However, dysregulated metabolism results in aberrant ROS production and altered redox balance, which in turn impinges upon the signal strength, thereby altering lineage choices of αβ and γδ T cells.